

Constraining the number of compact remnants near Sgr A*

Patrick Deegan and Sergei Nayakshin

Dept. of Physics & Astronomy, University of Leicester, Leicester, LE1 7RH, UK

13 September 2018

ABSTRACT

Due to dynamical friction stellar mass black holes and neutron stars are expected to form high density cusps in the inner parsec of our Galaxy. These compact remnants, expected to number around 20000, may be accreting cold dense gas present there, and give rise to potentially observable X-ray emission. Here we build a simple but detailed time-dependent model of such emission. We find that at least several X-ray sources of this nature should be detectable with *Chandra* at any one time. Turning this issue around, we also ask a question of what current observational constraints might be telling us about the total number of compact remnants. A cusp with ~ 40 thousand black holes over-predicts the number of discrete sources and the total X-ray luminosity of the inner parsec, and is hence ruled out. Future observations of the distribution and orbits of the cold ionised gas in the inner parsec of Sgr A* will put tighter constraints on the cusp of compact remnants.

Key words: Galaxy: centre – accretion: accretion discs – galaxies: active

1 INTRODUCTION

Theoretical calculations predict a cusp of around ~ 20000 stellar mass black holes in the central parsec of our Galaxy (Morris, 1993; Miralda-Escudé & Gould, 2000) and a similar number of neutron stars (Freitag et al., 2006; Hopman & Alexander, 2006). X-ray observations reveal a highly significant overabundance of transients in the same region (Muno et al., 2005) as compared with the region of \sim several tens of parsecs from Sgr A*, the $M_{\text{smbh}} \sim 4 \times 10^6 M_{\odot}$ super-massive black hole (Schödel et al., 2002; Ghez et al., 2003) in the Galactic Centre (GC). Nayakshin & Sunyaev (2006) proposed that these compact remnants may be accreting gas at relatively high rates when they happen to travel through a dense ionised gas observed to exist in the GC (also see Morris, 1993). They calculated a simple time-averaged model for X-ray emission from such a cusp, and concluded that the total emission of the cusp could be as high as $\gtrsim 10^{35}$ erg s $^{-1}$, i.e. very significant observationally.

On the other hand, a time-independent treatment does not do justice to the complexity of the problem. Despite the high total number of black holes, due to a small volume filling fraction of cold gas in the GC, only a few of the black holes will be moving within the gas clouds and possess a small enough relative velocity to be visible to *Chandra*. Here we extend the model of Nayakshin & Sunyaev (2006) in two ways. Firstly, we allow time-dependency in the problem by

explicitly following realistic Keplerian orbits of the compact objects. Secondly, we model the formation and evolution of small scale accretion discs around the accretors, as such discs will surely form due to an excess angular momentum in the accreting gas. Non-circular gas orbits are also considered with a simplified approach.

Our models show a large intrinsic time-dependence of the accretion on the compact objects and the X-ray emission it produces. Despite that, and despite internal uncertainties of the model (exact gas orbits, circularisation radius parameter, radiative efficiency, etc.), we feel that certain rather robust conclusions can be drawn. In particular, with the ~ 20000 compact remnants expected in the central parsec, at least several X-ray sources with X-ray luminosity greater than 10^{33} erg s $^{-1}$ should be present. Such sources, which can be called “fake X-ray binaries” for obvious reasons, can potentially contribute to the sources observed by Muno et al. (2005) in the central parsec. Conversely, it appears that a cusp significantly more populous, i.e., with 40000 compact remnants, would over-produce the X-ray emission as compared to the observations, and should thus be ruled out.

2 NUMERICAL APPROACH

The basis of our setup is explained in Nayakshin & Sunyaev (2006), and hence we shall only briefly discuss the main points, sparing detail for the improvements introduced here.

* E-mail: Sergei.Nayakshin at astro.le.ac.uk

We assume that a stellar mass black hole travelling through a gas cloud or a disc with density ρ is capturing gas in a *small scale disc about it* (see below) at the Bondi & Hoyle (1944) accretion rate:

$$\dot{M}_{\text{capt}} = 4\pi\rho \frac{(GM_{\text{bh}})^2}{(\Delta v^2 + c_s^2)^{3/2}}, \quad (1)$$

where c_s and Δv are the gas sound speed and the relative velocity between the black hole and the gas, respectively. The above picture is complicated by the presence of the SMBH. The area of influence of the stellar mass black holes is limited by the Hill's radius, $r_{\text{H}} = R(M_{\text{bh}}/3M_{\text{smbh}})^{1/3}$, where R is the distance between the stellar mass black hole and the SMBH. This imposes a limit on the capture rate, given by the Hill accretion rate, $\dot{M}_{\text{H}} = 4\pi r_{\text{H}}^2 \rho c_s$. Hence,

$$\dot{M}_{\text{capt}} = \min[\dot{M}_{\text{capt}}, \dot{M}_{\text{H}}] \quad (2)$$

where \dot{M}_{capt} on the right hand side of the equation is defined in eq.1.

2.1 Time-dependent disc accretion

The captured gas may have a net angular momentum resulting in the formation of a disk around the stellar mass black hole. The disc size is of order of the circularisation radius for the gas flow, r_c , which is unknown a priori. The maximum value of r_c is the capture radius, r_{capt} , which is

$$r_{\text{capt}} = \min \left[r_{\text{H}}, \frac{GM_{\text{bh}}}{\Delta v^2 + c_s^2} \right]. \quad (3)$$

We thus parametrise the circularisation radius as

$$r_c = \zeta r_{\text{capt}}, \quad (4)$$

where ζ is a parameter less than unity. The viscous time scale in such a disk around the stellar mass black hole is

$$t_{\text{visc}} = \frac{1}{\alpha\Omega_{\text{d}}} \left(\frac{r_{\text{capt}}}{h} \right)^2, \quad (5)$$

where α is the viscosity parameter, $\Omega_{\text{d}} = \sqrt{GM_{\text{bh}}/r_c^3}$ is the angular velocity of the disk and h is the height scale of the disk. Numerically,

$$t_{\text{visc}} = 1.5 \times 10^3 \text{ year } \alpha_{0.01}^{-1} \mu_{\text{d}} r_{\text{c},12}^{1/2} T_{\text{d},3}^{-1}, \quad (6)$$

where $T_{\text{d},3}$ is the disk temperature in units of 10^3 K, the viscosity parameter is $\alpha = 0.01\alpha_{0.01}$, μ_{d} is the mean molecular mass in units of Hydrogen mass and $r_{\text{c},12}$ is the circularisation radius in 10^{12} cm. This is to be compared with period (the orbital time) about the SMBH:

$$P = \frac{2\pi}{\Omega_{\text{K}}} = 2900 \text{ year } R_{0.1}^{3/2} M_6^{-1/2}. \quad (7)$$

Here, Ω_{K} is the Keplerian angular frequency for the black hole orbiting the super-massive one: $\Omega_{\text{K}} = \sqrt{GM_{\text{smbh}}/R^3}$. The respective Keplerian velocity is $v_{\text{K}} = R\Omega_{\text{K}}$.

Thus, the gas captured in the small scale disk accretes on the black hole after a delay of a fraction of to a few (black hole around the SMBH) orbital times. The evolution of the disk mass is given by the rate at which the mass is added, \dot{M}_{capt} , minus the mass accreted onto the black hole, \dot{M}_{acc} :

$$\frac{dM_{\text{d}}}{dt} = \dot{M}_{\text{capt}} - \dot{M}_{\text{acc}}. \quad (8)$$

The black hole accretion rate is calculated as

$$\dot{M}_{\text{acc}} = \frac{M_{\text{d}}}{t_{\text{visc}}} e^{-t_{\text{visc}}/12t} \quad (9)$$

(see §5.2 in Frank et al. (2002)). Finally, the luminosity of the accretion flow is modelled in the same way as in Nayakshin & Sunyaev (2006). Namely, we write $L_{\text{X}} = \epsilon \dot{M}_{\text{acc}} c^2$, where ϵ is given by

$$\epsilon = 0.01 \frac{\dot{M}_{\text{acc}}}{\dot{M}_0 + \dot{M}_{\text{acc}}}, \quad (10)$$

where $\dot{M}_0 = 0.01$ is the critical accretion rate where the switch from the radiatively efficient to radiatively inefficient regime occurs (Esin et al., 1997). Here we also assumed that X-ray emission visible in the *Chandra* band constitutes 10% of the bolometric efficiency, which would be a lower limit for typical spectra of X-ray binaries in their hard state.

2.2 Orbital evolution of accretors

We model the velocity and space distribution of stellar mass black holes as a cusp that follows the Bahcall & Wolf (1976) distribution for heavier species in a mass-segregated cusp. This distribution results in the black hole number density and velocity distribution obeying power laws of the form $R^{-7/4}$ and f_0 respectively, where,

$$f_0 \propto R^{-1/4} \left(1 - \frac{v^2}{v_{\text{esc}}^2} \right)^{-1/4}. \quad (11)$$

Both space and velocity distributions are isotropic. The most recent Monte-Carlo simulations Freitag et al. (2006) broadly support these classical results. A recent Fokker-Planck study (Hopman & Alexander, 2006) predicts a somewhat steeper power-law density dependence for the black hole cusp, $\rho_{\text{BH}} \propto R^{-2}$, but we leave this level of detail for future investigations.

Our black hole cusp is sharply cut at $R = 0.7$ pc (see Miralda-Escudé & Gould, 2000). Clearly, the artificial cut of the black hole distribution at the outer cusp radius is a crude approximation to the more complicated broken power-law structure of the cusp found by Freitag et al. (2006). It is also not entirely self-consistent as black holes do follow their orbits hence changing their radial position. To determine the significance of this we examined the structure of our model cusp in 10^4 years after it was set up. The density profile did in fact change. Some of black holes on eccentric orbits with large semi-major axes were found at radii much larger than the outer cusp radius assumed, as expected. However, the maximum change in the black hole density profile was no more than 30%. Furthermore, the black holes on very eccentric orbits will be those that accrete gas at a low rate unless gas in the inner parsec moves on similar eccentric orbits. Therefore emission from these black holes might be neglected in any event.

Generating a series of orbits consistent with this space-velocity distribution, we randomly set the initial phases of the black holes along their orbits, and then we follow their spatial motion. We also track the instantaneous gas capture rate for each black hole. When one of these orbits intersects the disc of the Minispiral, the black hole in question starts capturing gas and builds up a disc around it as described in §2.1.

Table 1. Orbital parameters of individual black hole orbits (see §3.1). The inclination of the orbit is with respect to the midplane of the Minispiral. The last column shows the time-averaged X-ray luminosity of the source.

Black hole	Inclination ($^{\circ}$)	Eccentricity	Semi-major axis (pc)	$\langle L_x \rangle$ erg s $^{-1}$
T1	6	0.1	0.1	1.78×10^{36}
T2	11	0.2	0.1	2.97×10^{34}
T3	1	0.6	0.3	1.34×10^{34}
T4	29	0.5	0.08	1.28×10^{32}

2.3 The model for the Minispiral

Paumard et al. (2004) suggests that the Minispiral is a dynamical feature in a state of almost a free fall onto Sgr A*. We feel that the Minispiral’s orbit is not likely to be so radial, as one would then expect Sgr A* itself to be accreting from the Minispiral. This would result in accretion rates far above that from the stellar winds (Cuadra et al., 2006), and would contradict the X-ray observations (e.g., Baganoff et al., 2003). More realistically the gas in the Minispiral follows an eccentric orbit which does not enter the inner arcsecond (~ 0.03 parsec) of the GC.

In our simple model, the Minispiral is modelled as half of a disc in a local Keplerian circular rotation around Sgr A* with the total gas mass of $M_{\text{disc}} = 50M_{\odot}$, in accord with estimates in Paumard et al. (2004). It extends from a radius of 0.1 pc from the SMBH to a radius of 0.5 pc. The disc heightscale, H , is assumed to have a fixed ratio to the radius, R : $H/R = 0.1$. The gas density is given by $\rho(R) = M_{\text{disc}}/(\pi R^2 H)$.

The dynamical age of the Minispiral is a few thousand years. Therefore, we ran our calculations for 3000 years with these assumptions, and then we “remove” the Minispiral instantaneously. This is done as a rough model of time evolution of the system in the case the gas apocenter is larger than 0.5 parsec, so that the Minispiral would leave the inner 0.5 parsec after a dynamical time. In §3.4 we vary some of the above assumptions about the structure of the Minispiral to estimate sensitivity of our results to these assumptions. In a future work a more complicated, but unavoidably model-dependent dynamic of the Minispiral should be included.

3 RESULTS

3.1 Emission from individual black holes

To motivate the study of X-ray emission from black hole cusps in this paper, we first examine the emission from individual black holes. For simplicity of discussion in this section only, the “half-disk” described in §2.3 is replaced with a full disk, with other parameters unchanged, the only exception being the mass of the Minispiral, which was doubled. The black holes follow Keplerian orbits (§2.2) that are characterised by the values of the semi-major axis and the eccentricity (see Table 1). The inclination of the orbit to

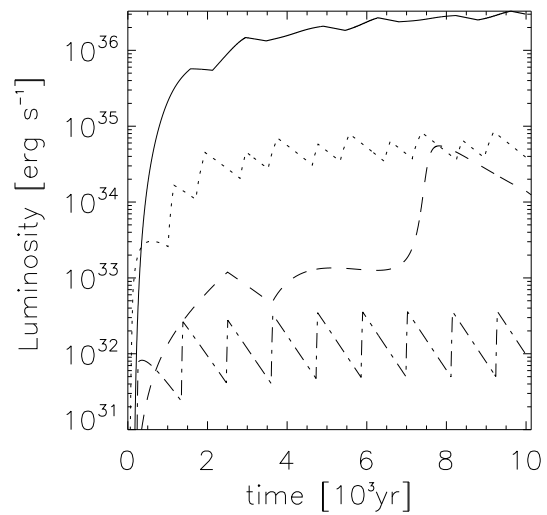


Figure 1. X-ray light curves of the four individual black holes described in §3.1; the solid, dotted, dashed and dotted-dashed lines correspond to T1, T2, T3, and T4 respectively.

the midplane of the disc, i , is also essential in determining the accretion history of the black hole in question. The orbital parameters of the test cases are summarised in Table 1. Figure 1 shows the resulting light curves for the four tests explored. The circularisation parameter is fixed at $\zeta = 0.1$ for all of the tests.

We start by looking at the most luminous case, T1 in Table 1, shown with the solid curve in Figure 1. Low inclination and eccentricity of the orbit ensure that the black hole spends all of its time inside the disc. In addition, the relative velocity between the black hole and the gas is small as the orbit of the former is close to circular. The capture rate is then large, resulting in a relatively high gas capture rate and X-ray luminosity. The few kinks in the lightcurve are caused by periodic variations in the relative velocity due to the eccentricity of the orbit. One could analyse these in terms of the epicyclic motion approximation for this nearly circular orbit.

The black hole in test T2 is on a slightly more eccentric and more inclined orbit. The relative black hole-gas velocity is larger than in test T1, and hence the gas capture rate (see eq. 1) is reduced. The black hole spends a significant amount of time inside the disc, but there are periods of time when it exits the disc through its one or the other face. Half of the dips in the lightcurve correspond to time spent outside the disc, and the other to the time when the relative velocity Δv reaches the highest value along the trajectory. Due to a relatively large size of the accretion disc (the “small scale” one discussed in §2.1) that builds up around the black hole, the viscous time is comparable to the duration of time spent outside of the disc, and hence the dips are relatively minor. The X-ray light curve of the source reaches a quasi-steady state with the luminosity $L_x \sim \text{few} \times 10^{34}$ erg s $^{-1}$ after $\sim 10^4$ years.

In test T3 we consider a black hole on a more eccentric

orbit, with eccentricity $e = 0.6$, and a larger semi-major axis. The high eccentricity of the orbit results in a high relative velocity which limits the gas capture rate. For most of the orbit, $L_X < 10^{33}$ erg s $^{-1}$. The luminosity of the black hole increases dramatically at $t \approx 8000$ years, when the black hole is at periastris, where the relative velocity is low enough and the density of the gas is high enough for the luminosity to approach that of case T2.

Finally test T4 is close to the worst case scenario as far as the gas capture rate is concerned. A high inclination and eccentricity orbit imply that the black hole spends little time inside the disc. Accumulation of gas in the small scale accretion disc happens in a burst-like manner when the black hole is inside the disc. Also note that since the relative velocity is high, gas capture radius (equation 3) is smaller than it is in tests T1 and T2, and hence the disc viscous time (equation 6) is shorter, resulting in shorter decay times for the “bursts” in the lightcurve. The X-ray luminosity is never larger than few $\times 10^{32}$ erg s $^{-1}$.

These simple tests indicate that we may expect the black holes to produce a detectable X-ray emission in one of the two ways: (i) a few black holes may be on orbits essentially co-moving with the gas, producing a few bright point sources; (ii) the dim majority of high inclination and/or high eccentricity orbits may not produce individually bright sources but may be collectively bright, producing an unresolvable “diffuse” X-ray emission.

3.2 Representative cases

Having considered the individual accretors case in the previous section we move on to the problem of the total black hole cusp emission with the Minispiral model as described in §2.3. The upper panels in Figure 2 display the total X-ray luminosity of a cluster of 5000 black holes as a function of time for two values of the circularisation radius parameter, ζ , 0.1 and 0.001, left and right, respectively. The lower panels show the number of X-ray sources with luminosity higher than 10^{33} erg s $^{-1}$ for the tests shown in the panels just above the respective lower panels. Such sources could be observed by *Chandra*. Several conclusions can be made. With a larger value of $\zeta = 0.1$, the accretion discs around black holes are larger, and thus viscous times are long. As a result, the X-ray emission varies smoothly with time, first increasing as the discs are built up, and then decreasing on \sim a thousand years time scale. Thus the sources are rather steady in time, and are also dim.

For the smaller value of $\zeta = 10^{-3}$, viscous times in small scale discs are much shorter. Therefore, the X-ray emission from the sources vary on much shorter time scales, i.e., of few years to tens of years. The sources are also brighter as the peak accretion rates are higher – each individual source shines much brighter for a shorter time, of course, as compared with the larger ζ case. Both the upper and the lower panels provide us with largely independent predictions which may be compared to X-ray observations.

Figure 3 shows the same experiments as Figure 2 but for 20000 black holes. Comparison between the two different values of ζ shows similar trends as before. It is interesting to compare the Figures 2 and 3. While the results depend significantly on the a priori unknown value of ζ , both low and high ζ tests show same tendency of a significant luminosity

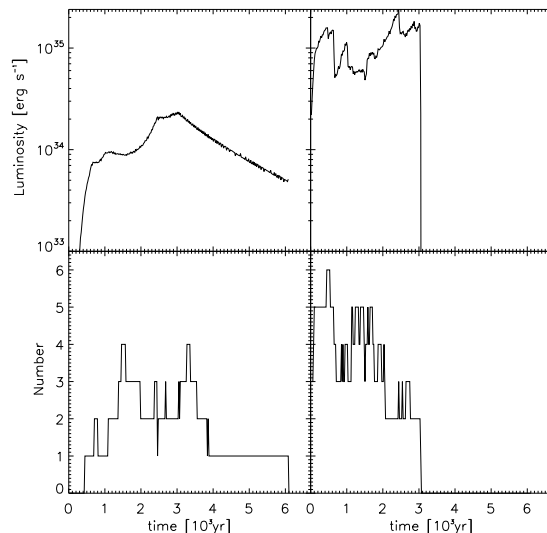


Figure 2. X-ray light curves (top panels) and number of individual sources (bottom panels) where $L_X < 10^{33}$ erg s $^{-1}$, when the total number of black holes in the inner parsec is 5000. The left and right panels correspond to $\zeta = 0.1$ and $\zeta = 0.001$ respectively.

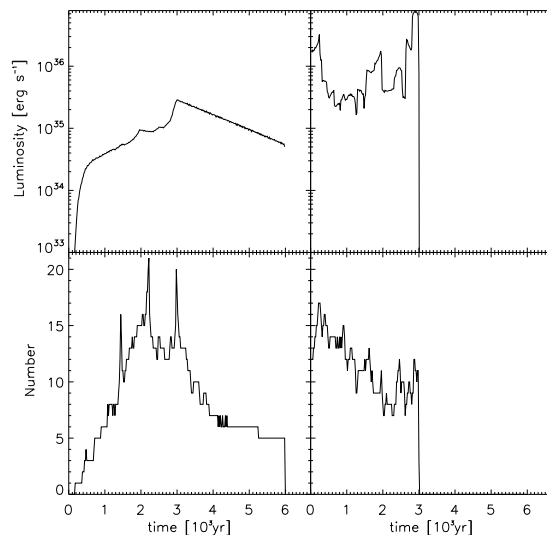


Figure 3. X-ray light curves and number of individual sources where $L_X < 10^{33}$ erg s $^{-1}$, when the total number of black holes in the inner parsec is 20000. The left and right panels correspond to $\zeta = 0.1$ and $\zeta = 0.001$ respectively.

increase with increase in the number of black holes. In fact, the luminosity increased by a larger factor than the black hole number did. The number of sources above the chosen luminosity threshold also increased. This suggests that by performing tests across all reasonable parameter space for ζ we should be able to find the maximum allowed number of stellar mass black holes in the cusp.

3.3 Search in the N , ζ parameter space

Following this idea, we ran a number of models for a range of values of ζ and for the total black hole numbers of $N = 5, 10, 20$ and 40 thousand. During the time period modelled, the results vary considerably in each test. For example, it is possible for just one single source to dominate the X-ray luminosity output of the cluster. In order to reduce and estimate statistical noise of the results, for each of the values of ζ and the total black hole number considered here, the tests were repeated three times, each time generating a new random black hole orbit distribution. We then calculate the mean value for the observables for the three runs, and we also find deviations from the mean values. The averaging is done between time $2000 < t < 3000$ years as to look at a state that may be similar to the present state of the Minispiral, given its estimated dynamical time.

A summary of the results is presented in Table 2. We chose to define several quantities. The most important are the average total X-ray luminosity of the black hole cluster and the number of black holes brighter than 10^{33} erg s $^{-1}$, N_X , as such sources would have been resolved by *Chandra* into separate point sources. Time-dependent variants of these quantities were plotted in Figures 2 and 3.

In addition to these, we defined the probabilities that the total luminosity of the cusp exceeds 10^{35} and 10^{36} erg s $^{-1}$ as the fraction of time these conditions are satisfied:

$$P(L_X > 10^{35}) = \frac{1}{t_f - t_i} \int_{L_X > 10^{35}} dt, \quad (12)$$

and obviously similarly for 10^{36} erg s $^{-1}$, t_i and t_f are 2000 and 3000 years respectively.

The probability of the number of individual sources brighter than $L_X > 10^{33}$ being larger than 3, 10 and 20 at a given time is defined in a similar way, e.g.,

$$P(N_X > 10) = \frac{1}{t_f - t_i} \int_{N_X > 10} dt. \quad (13)$$

These values can be compared to the number of discreet X-ray sources in the inner parsec as detected by *Chandra*.

Observations of the inner parsec by *Chandra* have placed upper limits on the total luminosity of sources of approximately 10^{35} erg s $^{-1}$ (Baganoff et al., 2003) and the number of individual X-ray sources with a luminosity greater than 10^{33} erg s $^{-1}$ of a dozen or so (F. Baganoff, private communication). With these constraints in mind we can immediately rule out the possibility that the cusp contains 40000 black holes. For any reasonable value of ζ , the total luminosity and the number of individual sources with $L_X > 10^{33}$ erg s $^{-1}$ are too large compared to observations. A cusp containing 20000 black holes is not very likely but cannot be ruled out completely at this time. In particular, only the larger ζ case is acceptable for $N = 20000$. Even though the average total cusp luminosity is $\sim 10^{36}$ erg s $^{-1}$ for this test, i.e., too large, the probability $P(L_X > 10^{35})$ is only ~ 0.66 . Cusps with $N = 5000$ or 10000 black holes is well within the limits imposed by observations.

3.4 Sensitivity of results to the properties of the Minispiral

We used a rather simple model for the Minispiral here (§2.3), partially because it is not yet clear what a better model for this gas would be. At the moment, we do not know the origin of this gaseous feature and the precise three-dimensional distribution of gas and velocity field (Paumard et al., 2004).

To test sensitivity of our conclusions to the properties of the Minispiral, we varied several of the assumptions made in §2.3. Table 3 summarises these tests. In particular, in one of the series of tests we let the Minispiral to be 3 times more massive, i.e., to contain $150 M_\odot$ of gas, with all other assumptions unchanged. In this case the luminosity of the cusp increases significantly at a given number of black holes, and even the $N = 10^4$ case is too luminous for the smaller values of the circularisation parameter ζ . Hence the upper limit on the number of black holes is then around 10^4 .

Another likely complication is that the gas may be on a parabolic or an eccentric trajectory rather than a circular one, as assumed in this paper until now. For such orbits, gas velocity can be both larger and smaller than the local Keplerian value, depending on where exactly on the orbit the gas is. Observationally, the Minispiral seems to be closer to the pericenter of its orbit rather than an apocenter (Paumard et al., 2004). To test the significance of non-Keplerian orbits, we let the gas velocity to be 1.2 and 1.4 times the local Keplerian value in the two series of tests presented in Table 3. Clearly this model is not geometrically self-consistent as the half-disc we use for the Minispiral should then deform in a complicated way, but we expect to gain some guidance to the direction of change in the results nonetheless. The larger gas velocity should result in a decrease in the number of black holes travelling at a low relative speed through the Minispiral, which should reduce the average gas capture rate (equation 1).

Table 3 shows that increasing the gas velocity to 1.2 of the local Keplerian value results in a marked drop in average luminosity of black holes, to the point that a cusp containing 40000 black holes cannot be ruled out for the larger value of the circularisation parameter, $\zeta = 0.1$. On the other hand, realistically, we would expect the sources to have a distribution in values of ζ , and we would thus expect a fair number of sources to have $\zeta \sim 0.01$ or less, which would then be ruled out.

Moving on to the gas velocity = $1.4v_K$, we note a further drop in the luminosity of the cusp and the number of sources detectable by *Chandra* (Table 3). Even the $N = 40000$ is allowed. We however feel that this model strongly over-simplifies the situation in the Galactic Centre. The Minispiral should be a feature bound to Sgr A* (or else the fact that it is crossing the innermost region of the parsec now would be a coincidence), and hence it is rather implausible that the gas is on a radial trajectory for which one would have $v = \sqrt{2}v_K \sim 1.4v_K$. We believe the case of $v = 1.2v_K$ is the one that represents the reality better.

Finally, the last entries in Table 3 are the tests with the Minispiral mass of $M = 150 M_\odot$ and $v = 1.2v_K$. A cusp of 40000 black holes is clearly inconsistent with the observations, whereas the $N = 20000$ is constrained but not completely ruled out.

3.5 A neutron star cusp

The mechanism that produces an overabundance of black holes in the Galactic Centre also applies to neutron stars, as they are also heavier than an average star. Simulations by Freitag et al. (2006) predict that a cusp of neutron stars will have a number density profile quite similar to that of stellar mass black holes. As far as our investigation goes, these neutron stars would be accreting gas in a similar manner to the black holes, with modifications only due to the smaller mass (we set $M_{\text{ns}} = 1.4 M_{\odot}$) and the existence of a surface.

We approximate the emission of an accreting neutron star as a black body one with temperature T_{ns} from the surface area $4\pi R_{\text{ns}}^2$, where $R_{\text{ns}} = 10$ km is the radius of the neutron star. Most of the radiation flux will be emitted at wavelengths corresponding to photon energy $E = 3kT_{\text{ns}}$:

$$E \approx 0.8 L_{34}^{1/4} \text{ KeV}, \quad (14)$$

where L_{34} is the X-ray Luminosity in units of $10^{34} \text{ erg s}^{-1}$. Due to the quite large absorbing column density to the GC, $N_{\text{H}} \sim 10^{23} \text{ cm}^{-2}$ (Baganoff et al., 2003), soft X-ray emission below ~ 1 keV is practically unobservable. We hence set the minimum observable total X-ray luminosity of a neutron star to be $10^{34} \text{ erg s}^{-1}$, rather than $10^{33} \text{ erg s}^{-1}$ for the black hole case.

We assume that the radiative efficiency of an accreting neutron star with negligible magnetic fields is constant at $\epsilon \sim 0.1$, in which case the luminosity of an accreting neutron star is simply

$$L_X = 0.1 \dot{M}_{\text{acc}} c^2. \quad (15)$$

Note that if magnetic fields are non-negligible, then the ‘‘propeller effect’’ may reduce the X-ray luminosity of neutron stars (Menou et al., 1999), but we leave these complications for a future more extended study.

With these modifications, we can use the machinery developed in §2 to calculate the X-ray emission from the cusp containing neutron stars. The results are presented in a way identical to the black hole cusp in Table 4. As with the black hole cusp case, the $N = 40000$ case is strongly ruled out on account of too large a number of detectable point sources, N_X , and the total X-ray luminosity of the cusp. The $N = 20000$ cusp also appears to be a bit too high in terms of both the total luminosity and the number of sources. The data may still be tolerable this, especially if one takes into account the possibility of the propeller effect (Menou et al., 1999) neglected here.

4 CONCLUSIONS

Stellar mass black holes and neutron stars are predicted to clutter the central parsec of our Galaxy (Morris, 1993; Miralda-Escudé & Gould, 2000; Freitag et al., 2006; Hopman & Alexander, 2006). While these predictions seem to be very robust, observational confirmation of the existence of a stellar remnant cusp is only indirect at the moment (Muno et al., 2005). Nayakshin & Sunyaev (2006) suggested that these sources, accreting *cold* gas episodically from the Minispiral or other molecular or ionised gas features found in the central parsec, may be bright both collectively and individually to be observable with *Chandra*. Here we presented a more

elaborated study, where a time-dependent disc accretion onto the compact sources was considered. Also, we took into account the fact that at low accretion rates, the radiative efficiency of black holes appears to be drastically reduced (e.g., Esin et al., 1997), and we used a Monte-Carlo like approach to randomly initialise the cusp of compact remnants.

The main effort in our paper was to set the upper limit on the number of compact remnants. Whereas the models have internal uncertainties, such as the value of circularisation parameter ζ , and observational uncertainties (the Mass and precise orbit of the Minispiral), a cusp of black holes or neutron stars with $N \gtrsim 40,000$ seems to be strongly ruled out. A cusp with $N \sim 20,000$ black holes, as theoretically predicted (Freitag et al., 2006; Hopman & Alexander, 2006), is broadly consistent with the data. Future efforts should improve these upper limits.

On the basis of our calculations, we think it is quite realistic that some of the X-ray sources visible in the central parsec (e.g., Baganoff et al., 2003; Muno et al., 2005) may be isolated black holes and neutron stars accreting gas from the Minispiral. Such sources should be preferentially found close to the Minispiral if viscous time is short (ζ is small). In addition, binary systems containing a black hole and a normal low mass star can also accrete gas in roughly the same way as we calculated here. In the case of low values of circularisation parameter, ζ , the size of the disc around the primary (the black hole) can be smaller than the size of the binary itself. Thus, these systems may appear as ‘‘fake X-ray binaries’’, where the gas supply comes from outside rather than from the low mass secondary. Observational signatures of such systems might be warped and out of binary plane accretion discs, ‘‘too short’’ or ‘‘too weak’’ accretion outbursts for the size of the binary.

We acknowledge stimulating discussions with Mark Freitag, Fred Baganoff and Rashid Sunyaev.

REFERENCES

- Baganoff F. K., Maeda Y., Morris M., et al., 2003, *ApJ*, 591, 891
 Bahcall J. N., Wolf R. A., 1976, *ApJ*, 209, 214
 Bondi H., Hoyle F., 1944, *MNRAS*, 104, 273
 Cuadra J., Nayakshin S., Springel V., Di Matteo T., 2006, *MNRAS*, 366, 358
 Esin A. A., McClintock J. E., Narayan R., 1997, *ApJ*, 489, 865
 Frank J., King A., Raine D. J., 2002, *Accretion Power in Astrophysics: Third Edition*, *Accretion Power in Astrophysics*, by Juhan Frank and Andrew King and Derek Raine, pp. 398. ISBN 0521620538. Cambridge, UK: Cambridge University Press, February 2002.
 Freitag M., Amaro-Seoane P., Kalogera V., 2006, *ArXiv Astrophysics e-prints*
 Ghosh A., Mo, B., Becklin, E., Duchêne G., et al., 2003, to be published in *Astron. Nachr.*, Vol. 324, No. S1 (2003), Special Supplement ‘‘The central 300 parsecs of the Milky Way’’, Eds. A. Cotera, H. Falcke, T. R. Geballe, S. Markoff, (astro-ph/0303151)
 Hopman C., Alexander T., 2006, *ApJL*, 645, L133
 Menou K., Esin A. A., Narayan R., Garcia M. R., Lasota J.-P., McClintock J. E., 1999, *ApJ*, 520, 276
 Miralda-Escudé J., Gould A., 2000, *ApJ*, 545, 847
 Morris M., 1993, *ApJ*, 408, 496

Table 2. Characteristics of black hole cusp averaged between 2000–3000 years (see §3.3).

Number ^a [10 ³]	ζ^b	$\langle L_X \rangle^c$ [10 ³⁵ erg s ⁻¹]	$P(L_X > 10^{36})^d$	$P(L_X > 10^{35})^e$	$\langle N_X \rangle^f$	$P(N_X > 20)^g$	$P(N_X > 10)^h$	$P(N_X > 3)^i$
5	0.001	1.85 ± 0.51	0	0.53 ± 0.5	2.76 ± 0.75	0	0.00 ± 0.00	0.33 ± 0.8
5	0.01	2.75 ± 1.33	0.42 ± 0.2	0.72 ± 0.1	4.2 ± 0.4	0	0	0.63 ± 0.13
5	0.1	0.73 ± 0.6	0	0.24 ± 0.3	2.23 ± 0.2	0	0	0.18 ± 0.11
10	0.001	15.91 ± 2.70	0.33 ± 0.13	0.90 ± 0.07	4.44 ± 0.28	0	0	0.71 ± 0.06
10	0.01	1.03 ± 0.24	0	0.45 ± 0.16	5.36 ± 0.26	0	0	0.90 ± 0.04
10	0.1	0.51 ± 0.28	0	0.31 ± 0.22	4.53 ± 1.52	0	0.01 ± 0.00	0.45 ± 0.21
20	0.001	19.97 ± 5.87	0.57 ± 0.05	0.99 ± 0.01	8.87 ± 0.81	0	0.19 ± 0.11	1.00 ± 0.00
20	0.01	9.67 ± 1.94	0.34 ± 0.14	0.99 ± 0.00	12.26 ± 1.40	0.01 ± 0.01	0.69 ± 0.17	1.00 ± 0.00
20	0.1	9.88 ± 4.49	0.34 ± 0.22	0.66 ± 0.23	13.11 ± 1.25	0.01 ± 0.00	0.74 ± 0.16	1.00 ± 0.00
40	0.001	40.37 ± 1.75	1.00 ± 0.00	1.00 ± 0.00	19.40 ± 0.37	0.34 ± 0.05	1.00 ± 0.00	1.00 ± 0.00
40	0.01	100.53 ± 62.13	0.77 ± 0.08	0.99 ± 0.00	24.66 ± 0.50	0.85 ± 0.05	1.00 ± 0.00	1.00 ± 0.00
40	0.1	6.50 ± 1.83	0.20 ± 0.14	1.00 ± 0.00	24.59 ± 2.18	0.72 ± 0.14	1.00 ± 0.00	1.00 ± 0.00

The columns list:

^a Total number of black holes in the cusp

^b Circularisation parameter (§2.1)

^c Time-averaged luminosity of the cusp

^{d-e} Probability that the total luminosity of the cusp is greater than 10³⁶ or 10³⁵ erg s⁻¹, respectively.

^f Average number of sources with X-ray luminosity greater than 10³³erg s⁻¹(N_X)

^{g-i} Probability that N_X is greater than 20, 10 and 3, respectively

Muno M. P., Pfahl E., Baganoff F. K., et al., 2005, ApJL, 622, L113

Nayakshin S., Sunyaev R., 2006, ArXiv Astrophysics e-prints

Paumard T., Maillard J.-P., Morris M., 2004, A&A, 426, 81

Schödel R., Ott T., Genzel R., et al., 2002, Nature, 419, 694

Table 3. Same as Table 2, but for different models of the Minispiral

Number [10^3]	ζ	$\langle L_X \rangle$ [$10^{35} \text{erg s}^{-1}$]	$P(L_X > 10^{36})$	$P(L_X > 10^{35})$	$\langle N_X \rangle$	$P(N_X > 20)$	$P(N_X > 10)$	$P(N_X > 3)$
3 Mgas^a								
5	0.01	28.13 ± 11.54	0.62 ± 0.15	0.84 ± 0.08	5.81 ± 0.95	0	0.03 ± 0.02	0.84 ± 0.06
5	0.1	1.53 ± 4.45	0	0.67 ± 0.40	7.04 ± 0.47	0	0.06 ± 0.04	1.00 ± 0.00
10	0.01	35.21 ± 12.01	0.63 ± 0.17	1.00 ± 0.00	9.24 ± 0.93	0	0.36 ± 0.13	1.00 ± 0.00
10	0.1	2.06 ± 0.74	0	0.56 ± 0.16	14.12 ± 0.51	0.02 ± 0.00	0.98 ± 0.01	1.00 ± 0.00
20	0.01	24.53 ± 6.02	0.77 ± 0.13	1.00 ± 0.00	18.95 ± 1.25	0.40 ± 0.16	1.00 ± 0.00	1.00 ± 0.00
20	0.1	5.47 ± 0.41	0.01 ± 0.00	1.00 ± 0.00	29.38 ± 2.06	0.90 ± 0.07	1.00 ± 0.00	1.00 ± 0.00
1.2v_K^b								
5	0.01	0.93 ± 0.55	0.02 ± 0.01	0.14 ± 0.07	1.85 ± 0.36	0	0	0.10 ± 0.04
5	0.1	0.05 ± 0.03	0	0	0.44 ± 0.20	0	0	0
10	0.01	0.45 ± 0.10	0	0.13 ± 0.05	3.47 ± 0.42	0	0	0.49 ± 0.13
10	0.1	0.38 ± 0.25	0	0.17 ± 0.12	2.45 ± 1.42	0	0	0.31 ± 0.22
20	0.01	4.86 ± 1.63	0.14 ± 0.05	0.43 ± 0.15	6.65 ± 0.08	0	0.03 ± 0.01	0.91 ± 0.04
20	0.1	0.35 ± 0.07	0	0	4.24 ± 0.08	0	0	0.76 ± 0.07
40	0.01	40.65 ± 1.66	0.56 ± 0.14	0.94 ± 0.04	13.42 ± 0.23	0.02 ± 0.01	0.74 ± 0.06	1.00 ± 0.00
40	0.1	1.05 ± 0.37	0	0.18 ± 0.13	10.27 ± 0.62	0	0.44 ± 0.80	1.00 ± 0.00
1.4 v_K^c								
5	0.01	0.07 ± 0.02	0	0	0.71 ± 0.15	0	0	0
5	0.1	0.02 ± 0.00	0	0	0.37 ± 0.26	0	0	0
10	0.01	0.12 ± 0.04	0	0	1.17 ± 0.21	0	0	0
10	0.1	0.05 ± 0.01	0	0	0.83 ± 0.32	0	0	0
20	0.01	0.32 ± 0.48	0	0.03 ± 0.02	3.66 ± 0.43	0	0	0.49 ± 0.13
20	0.1	0.03 ± 0.00	0	0	0.11 ± 0.05	0	0	0
40	0.01	0.64 ± 0.14	0	0.18 ± 0.09	5.37 ± 0.60	0	0.04 ± 0.01	0.72 ± 0.07
40	0.1	0.12 ± 0.03	0	0	1.34 ± 0.36	0	0	0.01 ± 0.01
3 Mgas & 1.2 v_K^d								
20	0.01	9.79 ± 0.93	0.34 ± 0.06	1.00 ± 0.00	15.47 ± 0.25	0.07 ± 0.02	0.98 ± 0.01	1.00 ± 0.00
20	0.1	2.89 ± 1.03	0.09 ± 0.06	0.86 ± 0.10	13.72 ± 0.25	0.04 ± 0.01	0.91 ± 0.03	1.00 ± 0.00
40	0.01	12.17 ± 0.96	0.59 ± 0.02	1.00 ± 0.00	25.02 ± 0.78	0.90 ± 0.05	1.00 ± 0.00	1.00 ± 0.00
40	0.1	6.43 ± 1.76	0.29 ± 0.10	0.93 ± 0.05	19.63 ± 1.82	0.50 ± 0.16	1.00 ± 0.00	1.00 ± 0.00

^a Mass of the Minispiral has been tripled to $150 M_\odot$ ^b Velocity of the gas has been increased to $1.2 v_K$, where v_K is the local keplerian velocity^c Velocity of the gas has been increased to $1.4 v_K$ ^d Mass of the Minispiral has been tripled to $150 M_\odot$ and the velocity of the gas has been increased to $1.2 v_K$

Table 4. Same as Table 2 but for a neutron star cusp.

Number ^a [10 ³]	ζ^b	$\langle L_X \rangle^c$ [10 ³⁵ erg s ⁻¹]	P($L_X > 10^{36}$) ^d	P($L_X > 10^{35}$) ^e	$\langle N_X \rangle^f$	P($N_X > 20$) ^g	P($N_X > 10$) ^h	P($N_X > 3$) ⁱ
5	0.001	3.23 ± 5.24	0.08 ± 0.06	0.79 ± 0.11	2.84 ± 0.43	0	0	0.32 ± 0.10
5	0.01	2.43 ± 0.76	0	0.67 ± 0.12	2.78 ± 0.81	0	0	0.38 ± 0.16
5	0.1	1.44 ± 0.18	0	0.85 ± 0.11	2.90 ± 0.67	0	0	0.34 ± 0.20
10	0.001	4.17 ± 0.90	0.02 ± 0.01	0.99 ± 0.01	6.25 ± 0.45	0	0.03 ± 0.02	0.94 ± 0.02
10	0.01	5.89 ± 1.38	0.18 ± 0.08	0.99 ± 0.01	4.53 ± 0.34	0	0	0.72 ± 0.10
10	0.1	6.69 ± 3.59	0.30 ± 0.21	0.83 ± 0.12	3.32 ± 0.15	0	0	0.47 ± 0.05
20	0.001	8.13 ± 1.34	0.27 ± 0.11	1.00 ± 0.00	11.52 ± 1.15	0	0.57 ± 0.15	1.00 ± 0.00
20	0.01	9.73 ± 1.73	0.32 ± 0.12	1.00 ± 0.00	7.32 ± 0.30	0	0.11 ± 0.08	0.97 ± 0.02
20	0.1	7.17 ± 2.15	0.27 ± 0.19	1.00 ± 0.00	9.00 ± 0.35	0	0.19 ± 0.05	1.00 ± 0.00
40	0.001	41.60 ± 12.71	0.99 ± 0.01	1.00 ± 0.00	21.99 ± 0.52	0.69 ± 0.07	1.00 ± 0.00	1.00 ± 0.00
40	0.01	18.62 ± 4.46	0.87 ± 0.07	1.00 ± 0.00	15.82 ± 0.48	0.04 ± 0.02	0.99 ± 0.00	1.00 ± 0.00
40	0.1	17.91 ± 3.74	0.86 ± 0.10	1.00 ± 0.00	21.34 ± 0.34	0.66 ± 0.05	1.00 ± 0.00	1.00 ± 0.00

^a - ^e see Table 2 caption.

^f Average number of neutron stars with L_X greater than 10^{34} erg s⁻¹(N_X). Only sources with $L_X > 10^{34}$ are visible, see §3.5.

^g - ⁱ see Table 2 caption.